27. A NUMERICAL TECHNIQUE FOR ANALYSIS OF WAVE DRAG AT LIFTING CONDITIONS

By Roy V. Harris, Jr.
NASA Langley Research Center

SUMMARY

A numerical technique for an application of the far-field linear theory is presented. This technique, when adapted to the high-speed electronic digital computer, provides a practical means for analyzing the total wave drag of an airplane at lifting conditions. An indication of the accuracy of the method at lifting conditions is shown by comparing measured pressure signatures at various azimuth angles about an airplane model with those predicted by theory. Calculations are made to illustrate some effects of configuration variables on the total wave drag of an airplane at lifting conditions.

INTRODUCTION

The recent development of numerical techniques for estimating and optimizing the lift-drag characteristics of supersonic cruise vehicles has led to significant improvements in aerodynamic performance at supersonic speeds (ref. 1). Most of these techniques have resulted from applications of existing theories to the high-speed electronic digital computer. As a result, analytical approaches which once were considered too complex for practical application can now be used to conduct aerodynamic trade studies in time to affect the preliminary design of airplanes.

Two approaches to the analytical drag buildup of an airplane at supersonic speeds are illustrated in figure 1. On the left of the figure is an illustrative drag polar for a supersonic-cruise vehicle with the cruise lift coefficient indicated by the solid symbol. For purposes of analysis, the drag is usually considered to be composed of skin-friction drag, zero-lift wave drag (or wave drag due to volume), and drag due to lift. This approach to the drag calculation was used in paper no. 26 by Harry W. Carlson and F. Edward McLean. It should be noted, however, that the drag due to lift consists of part vortex drag and part wave drag due to lift, and that the approach utilized by Carlson and McLean neglects any interference effects between the wave drag due to lift and that due to volume. A more fundamental approach, as illustrated by the bar graph on the right, is to consider the drag to be composed of its three basic elements, friction drag, total wave drag (including that due to lift), and vortex drag. Some aspects of the techniques for calculating skin-friction drag are discussed in paper no. 30. by John B. Peterson, Jr., and William J. Monta and in paper no. 31 by K. R. Czarnecki. The calculation of vortex drag at supersonic speeds for the condition of 100 percent leading-edge suction is the same as the

calculation of induced drag at subsonic speeds and depends only on the spanwise load distribution (ref. 2). For the more realistic condition in which little or no leading-edge suction is achieved at supersonic speeds, the problem is more complex and no suitable numerical technique presently exists. A numerical technique has been developed for the analysis of airplane wave drag at lifting conditions, and the purpose of this paper is to present this new application of the far-field linear theory which, when adapted to the high-speed electronic digital computer, provides a practical means for analyzing the total wave drag of an airplane at lifting conditions.

SYMBOLS

A	equivalent-body area due to volume
C_D	total-drag coefficient
$C_{D,wave}$	wave-drag coefficient
C_L	lift coefficient
D	wave drag
l	component of section lift along intercept of airplane and the Mach cutting plane, taken in direction of θ
L	length of equivalent body
M	Mach number
p	reference static pressure
Δp	incremental pressure due to flow field of airplane or model
q	dynamic pressure
S	total equivalent-body area
x,y,z	coordinates along X, Y, and Z axes
X,Y,Z	axis system of airplane or model
$\beta = \sqrt{M^2 - 1}$	
θ	azimuth angle referred to control cylinder, as shown in figure 2
μ	Mach angle

Primes are used to indicate derivatives with respect to x.

DISCUSSION

Calculation of Wave Drag at Lifting Conditions

The far-field linear-theory approach to supersonic flow is illustrated in figure 2. Consider an airplane in a steady supersonic stream and the cylindrical control volume suggested by Hayes in reference 2. Define the azimuth angle θ to be such that θ is zero to the side of the airplane, with negative values below the airplane and positive values above it. Consider next a point on the surface of the control volume below the airplane and between the forward and rearward trailing Mach cones. The upstream Mach forecone from this point represents a surface of coincident signals in that all disturbances which lie in this plane arrive at the point simultaneously. It is possible, therefore, to determine a linear distribution of singularities that produce the same pressure disturbances as the airplane at the surface of the control volume. If the dimensions of the control volume are allowed to become infinitely large, the surfaces of coincident signals become planes in the vicinity of the airplane, and the linear source-sink distribution can be related to an equivalent-body area distribution (shown in fig. 2), which is determined by the intercepts of the planes of coincident signals (referred to as the "Mach cutting planes") and the airplane. The dotted lines shown in the area-distribution sketches indicate the equivalent-body area distribution due to volume and the solid lines indicate the total equivalent-body area distribution including the effects of lift.

The mathematical basis for the concept of equivalent area due to lift can be determined from the following equation for airplane wave drag (refs. 2 and 3) that was derived by use of the far-field linear-theory approach:

$$\frac{D}{q} = \frac{-1}{4\pi^2} \int_0^{2\pi} \int_0^L \int_0^L \left[A''(x_1,\theta) - \frac{\beta}{2q} l'(x_1,\theta)\right]\left[A''(x_2,\theta) - \frac{\beta}{2q} l'(x_2,\theta)\right] \log_e |x_1 - x_2| \, dx_1 \, dx_2 \, d\theta$$

This equation shows that the ratio of the wave drag to the free-stream dynamic pressure is a function of the second derivative of the equivalent-body area distribution due to volume $A(x,\theta)$ and is also a function of a term that is proportional to the first derivative of the longitudinal distribution of lift $l(x,\theta)$, as determined by the Mach cutting planes. If the term $S(x,\theta)$ is so defined that

$$S''(x,\theta) = A''(x,\theta) - \frac{\beta}{2q} l'(x,\theta)$$

then

$$S(x,\theta) = A(x,\theta) - \frac{\beta}{2q} \int_0^x l(x,\theta)dx$$

It can thus be seen that $S(x,\theta)$ is equal to the equivalent-body area distribution due to volume minus a term which has units of area and is a function of the longitudinal lift distribution as determined by the Mach cutting planes. This term is defined as the equivalent-body area due to lift. As illustrated in figure 2, the equivalent-body area due to lift varies from positive values below the airplane to negative values above the airplane. To the side of the airplane, the area due to lift becomes zero since there is no component of lift in this direction. It should be noted that the pressures that occur below the airplane cause the sonic boom along the ground track. Also, the equivalent-body area distribution corresponding to $\theta = -90^\circ$ is used in the calculation of sonic-boom signatures. This subject is treated subsequently in paper no. 29 by McLean, Carlson, and Hunton.

An illustration of the procedure that has been programed for determining the equivalent-body area distributions of an airplane at lifting conditions is presented in figure 3. The left side of the figure illustrates the procedure for determining the area due to volume and the right side of the figure illustrates the procedure used to determine the area due to lift. For calculation of the equivalent-body area due to volume, a mathematical representation of the airplane in terms of the x, y, and z coordinates is used as input to the computer. The computer then solves for the normal projection of the area intercepted by the Mach cutting planes and thus defines the equivalent-body area due to volume $A(x,\theta)$. For calculation of the equivalent-body area due to lift, the wing camber surface in terms of x, y, and z coordinates is used as input to the computer, and the lifting-surface pressure distribution is determined by the method which was described in paper no. 26 by Carlson and McLean. The computer then solves for the intercept of the Mach cutting planes and the wing camber surface and integrates the lifting pressures along this line to determine the component of force normal to the free stream and in the θ direction. This component of force $l(x,\theta)$ is then used to define the equivalent-body area due to lift. Finally, the computer sums the area due to volume and the area due to lift and solves for the total wave drag.

Direct comparisons between measured and computed wave drag at lifting conditions cannot be made because of the difficulty in determining the supersonic vortex drag. Numerous correlations at zero lift, however, have shown good agreement with the theory (ref. 4). An indication of the accuracy of the equivalent-body concept at lifting conditions can be made by comparing the measured pressure signatures at various azimuth angles about an airplane model with those predicted from its equivalent bodies. Such a comparison is made in figure 4. These data were taken at a Mach number of 1.4 and a lift coefficient of 0.10 for the configuration shown in the sketch. The upper three plots show the equivalent-body area distributions for the azimuth angle of -90° (which is directly below the model), the azimuth angle of 0° (which is to the side), and the azimuth angle of 90° (which is above the model). The dashed lines indicate the area due to volume and the solid lines indicate the total equivalent-body area including the effects of lift. The three corresponding lower plots show a comparison between the pressure signatures predicted by theory and those measured in the wind-tunnel tests. The classic far-field type of pressure signature was not achieved in these tests because of the dimensional restraints imposed by the wind tunnel. The near-field effects have been included,

however, in the theoretical predictions (ref. 5). The good agreement between the measured and predicted pressure signatures at the various azimuth angles indicates that good agreement for the wave drag at lift should be expected.

Calculations of the wave drag at several lifting conditions have been made for the configuration shown in figure 4 at a Mach number of 2.7, and some of the results are shown in figure 5. The upper plots show the equivalent-body area distributions for lift coefficients of 0 and 0.08. The lower plots show the corresponding ratio of the equivalent-body wave drag to dynamic pressure as a function of the azimuth angle. The dashed lines indicate the integrated average and, hence, the total wave drag of the airplane. Consider, first, the results at zero lift for which the entire equivalent-body area is due to volume and, therefore, only positive areas exist. This portion of the figure is simplified by showing only selected area distributions for positive values of the azimuth angle. Comparing the shape of each equivalent-body area distribution with its corresponding drag contribution in the lower plot indicates that the equivalent bodies having the lowest fineness ratios and the steepest slopes make the largest contribution to the wave drag. For example, the equivalent body for an azimuth of 90° has the largest maximum area and the shortest length and, therefore, the largest contribution to the wave drag of the airplane. At a lift coefficient of 0.08, the area due to lift significantly alters the shape of the equivalent-body area distributions. The equivalent body for an azimuth of 90°, for example, although having the same length as the zero-lift condition, now has a much larger area change occurring over that length and therefore makes a much larger contribution to the airplane wave drag. Thus, a direct relationship can be established between the wave drag of an airplane at any given lift coefficient and its equivalent-body area distributions.

Configuration Effects on Wave Drag at Lifting Conditions

A comparison of the wave drag of two similar configurations at a Mach number of 2.0 and a lift coefficient of 0.10 is shown in figure 6. Both wing-body combinations were symmetrical, employed the same body, and had wings of equal area, equal span, and equal thickness ratio. One configuration, however, had a wing of delta planform, whereas the other had a wing of arrow planform. Comparing the equivalent-body area distributions at azimuth angles of -90°, 0°, and 90° indicates that the effect of spreading the lift over a greater length with the arrow wing is to reduce the rate of area growth of the equivalent bodies. The effect on the airplane wave drag is shown in the lower plots, where the total wave drag of the arrow-wing configuration is about 30 percent less than that of the delta-wing configuration.

Up to this point, all configurations that have been considered would be expected to have little or no interference between wave drag due to lift and wave drag due to volume. An example for which interference effects do exist between wave drag due to lift and that due to volume is shown in figure 7. Consider the arrow-wing—body configuration shown in figure 6, again at a Mach number of 2.0 and a lift coefficient of 0.10, but now with a high wing position as shown at the left in figure 7 and with a low wing position as shown at the right. The equivalent-body area distribution for $\theta = 0°$ (which is to the

side of the airplane) is unaffected by changes in the vertical position of the wing and, thus, is the same for both configurations. The Mach cutting planes intercept the high-wing configuration in such a manner that the area due to lift is shifted forward to the center line for the azimuth angle of 90° and is shifted rearward for the azimuth angle of -90°. For the low-wing configuration, the reverse is true. The area due to lift is shifted rearward for an azimuth angle of 90° and forward for an azimuth angle of -90°. The effects of interference between lift and volume on the total wave drag can be seen in figure 8. The bar graph shows a comparison of total wave-drag coefficient based on wing area for the low-wing, midwing, and high-wing configurations. For this example, the low-wing arrangement results in a 7.5 percent higher wave drag than the high-wing arrangement.

CONCLUDING REMARKS

A numerical technique has been presented for an application of the far-field linear theory. This technique, when adapted to the high-speed electronic digital computer, provides a practical means for analyzing the total wave drag of an airplane at lifting conditions. Numerous correlations at zero lift have shown good agreement with the theory. An indication of the accuracy of the method at lifting conditions was shown by comparing measured pressure signatures at various azimuth angles about an airplane model with those predicted by theory. The good agreement between the measured and predicted pressure signatures indicates that good agreement for the wave drag at lifting conditions should be expected. Results from a limited number of calculations showed some effects of differences in configuration on the total wave drag of airplanes at lifting conditions.

REFERENCES

1. Robins, A. Warner; Morris, Odell A.; and Harris, Roy V., Jr.: Recent Research Results in the Aerodynamics of Supersonic Vehicles. Paper No. 65-717, Am. Inst. Aeron. Astronaut., Nov. 1965.

2. Hayes, Wallace D.: Linearized Supersonic Flow. Rept. No. AL-222, North American Aviation, Inc., June 18, 1947.

3. Lomax, Harvard: The Wave Drag of Arbitrary Configurations in Linearized Flow as Determined by Areas and Forces in Oblique Planes. NACA RM A55A18, 1955.

4. Harris, Roy V., Jr.: An Analysis and Correlation of Aircraft Wave Drag. NASA TM X-947, 1964.

5. Middleton, Wilbur D.; and Carlson, Harry W.: A Numerical Method for Calculating Near-Field Sonic-Boom Pressure Signatures. NASA TN D-3082, 1965.

TWO APPROACHES TO ANALYTICAL DRAG BUILDUP

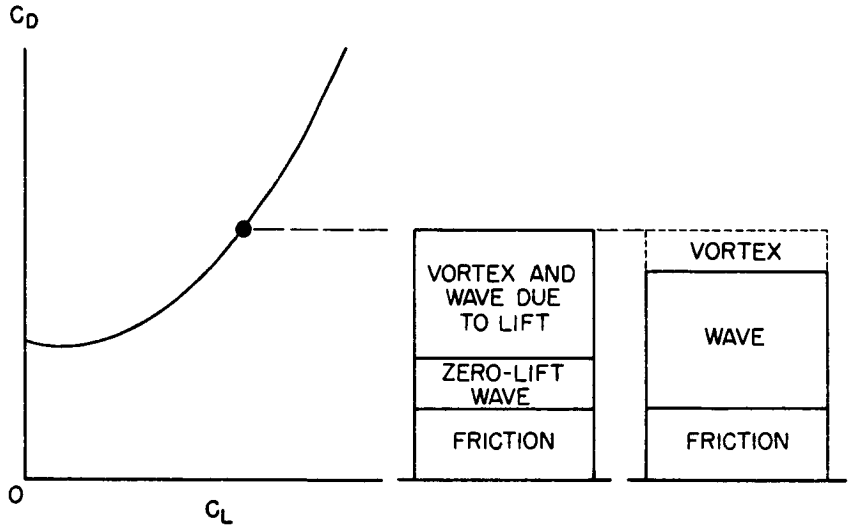

Figure 1

ILLUSTRATION OF FAR-FIELD LINEAR-THEORY APPROACH

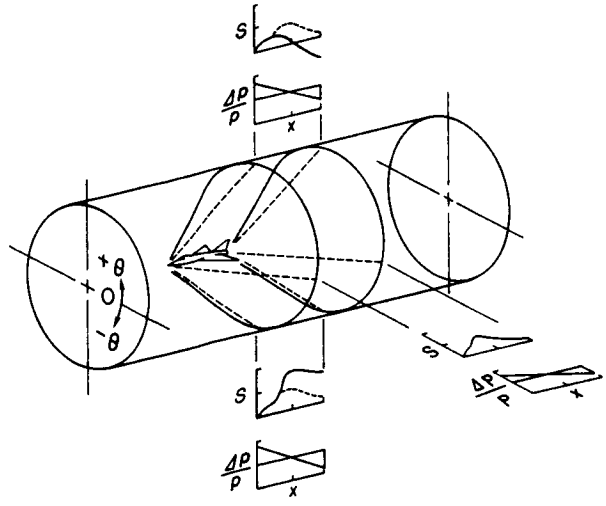

Figure 2

ILLUSTRATION OF MACHINE COMPUTING PROCEDURE

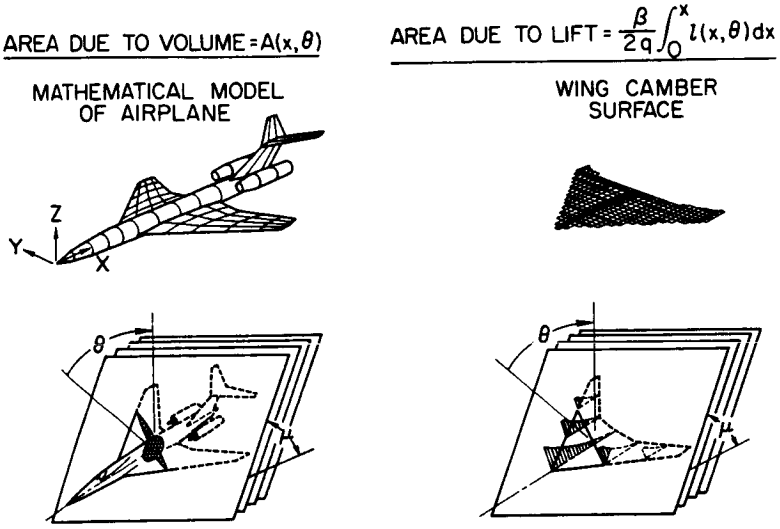

Figure 3

EXPERIMENTAL VERIFICATION OF EQUIVALENT-BODY CONCEPT

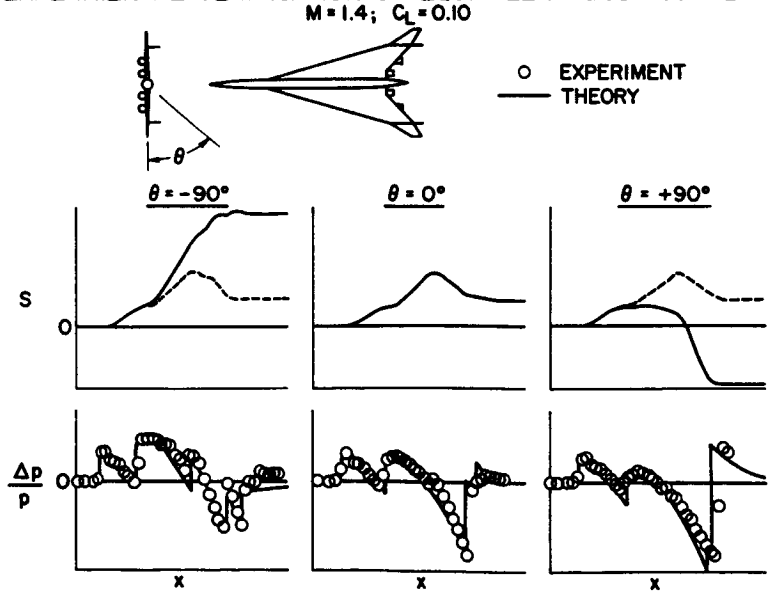

Figure 4

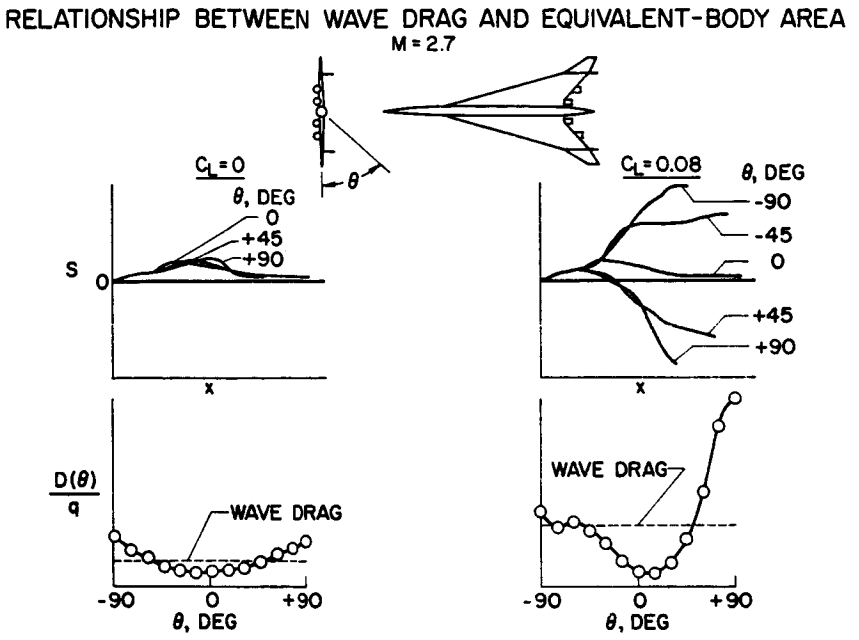

Figure 5

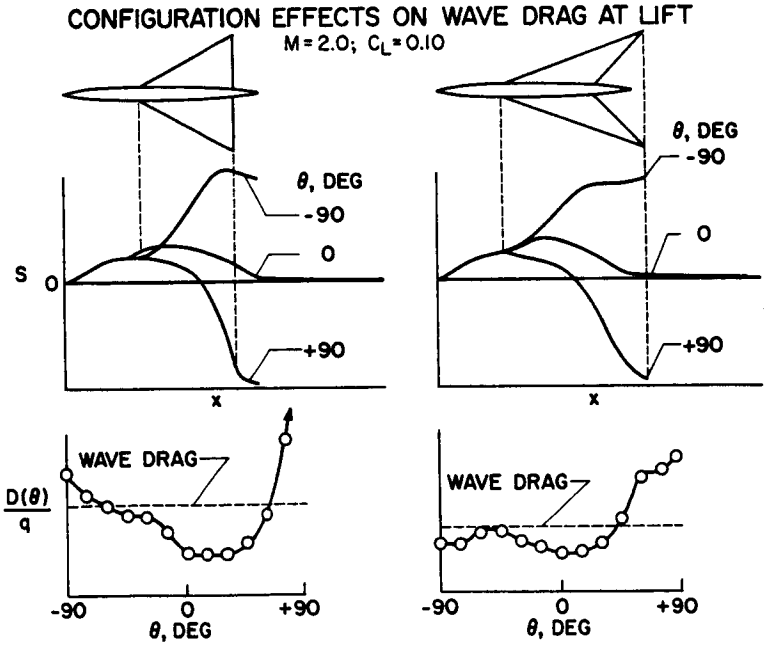

Figure 6

INTERFERENCE EFFECTS BETWEEN LIFT AND VOLUME
AREA DISTRIBUTIONS AT M=2.0 AND C_L=0.10

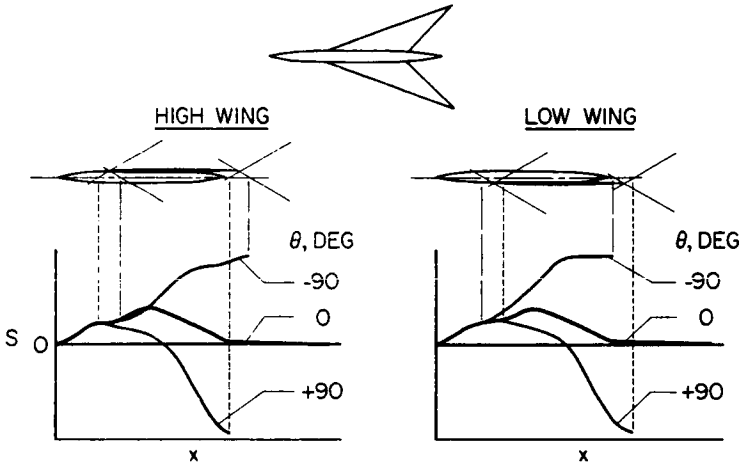

Figure 7

INTERFERENCE EFFECTS BETWEEN LIFT AND VOLUME
WAVE DRAG AT M=2.0 AND C_L=0.10

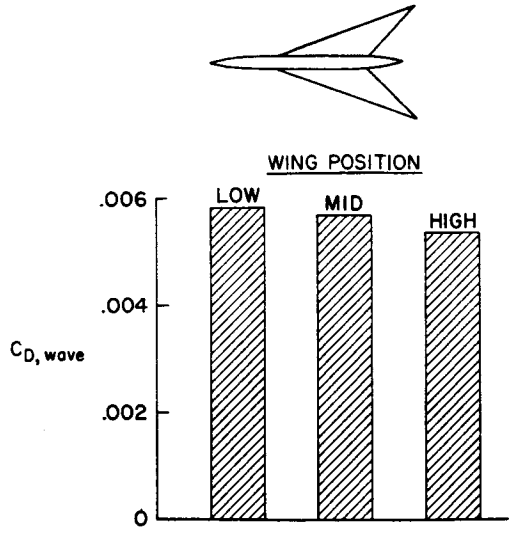

Figure 8